Determination of radiation couplings in climate change simulations: Analysis with two different linearization methods

Martin, A.[1,*]**, Quaas, J.**[1]

[1]) *Institute for Meteorology, Stephanstr. 3, 04103 Leipzig,*
E-Mail: a.martin@mpic.de
[*]) *Now at: Max-Planck-Institut for Chemistry, Hahn-Meitner-Weg 1, 55128 Mainz*

Zusammenfassung: In dieser Arbeit werden zwei Linearisierungsmethoden zur Bestimmung von Strahlungskopplungen in Klimaänderungssimulationen verglichen. Die individuellen Feedbackparameter werden mit der Partial Radiative Perturbation (PRP)-Methode und der Kernel Methode basierend auf CMPI6 Daten des Max-Planck-Instituts Earth System Model in Low Resolution (MPI-ESM-LR) mit vierfacher CO_2-Konzentration berechnet. Für die Berechnung der Feedbacks wurde das eigenständige ECHAM6 Strahlungsmodul genutzt. Neben regionalen Besonderheiten der einzelnen Rückkopplungsparameter, zeigen sich die größten Unterschiede im Oberflächenalbedo Feedback. Wasserdampf, Lapses-Rate und Planck Feedback weisen eine vergleichsweise geringe Methodenabhänigkeit auf. Dies kann auch im Vergleich mit vorherigen Studien verifiziert werden. Zusätzlich wird gezeigt, dass die Verwendung von mehrjährigen Monatsmittelwerten den Rechenaufwand bei nur geringem Genauigkeitsverlust reduziert.

Summary: In this paper two linearization methods for the determination of radiation couplings in climate change simulations are compared. Individual feedback parameters are calculated using the partial radiative perturbation (PRP) method and kernel-technique based on CMIP6 data of the Max Planck Institute Earth System Model at Low Resolution (MPI-ESM-LR) model with quadrupled CO_2 concentration. The applied kernels were computed separately for two directions using the same radiation module as for the PRP method, providing the opportunity to compare both based on the same data basis. The largest disagreements between methods were found for the surface albedo feedback, followed by the water vapor feedback, lapse-rate feedback and Planck feedback, whereas the differences of the last three mentioned are minor. Nevertheless, the found results are within the range of former studies. Beside regional features of the individual feedback parameters, an overall good agreement between the PRP and kernel approach is observed. Additionally, it is shown that the use of multiyear monthly averages reduces the computational expense with only a small loss in accuracy, compared to calculations based on yearly monthly averages.

1 Introduction

Climate and the earth's atmospheric composition are continuously changing. Thus, the analysis and simulation of changes in atmospheric composition is of great importance

to obtain possible impacts on the global climate. In this context, the fraction of greenhouse gases in the atmosphere plays a significant role. Consequently, many studies have been conducted on the effect of increased CO_2 levels and their impact on global surface temperature. The change in mean global surface temperature due to a doubling in CO_2 within the atmosphere is the so-called equilibrium climate sensitivity. Currently, the fifth Assessment Report of the Intergovernmental Panel on Climate Change (IPCC AR5) estimates the equilibrium climate sensitivity (ECS) in the range of $3.2 \pm 1.3\,^{\circ}\mathrm{C}$ (Flato et al. 2013). The variability of the ECS is strongly related to physical adjustment processes, so-called climate feedbacks. The characterization of those climate feedbacks, in terms of order of magnitude and sign are especially relevant for global climate model evaluations. In the following the PRP method and the radiative kernel technique are applied to identify possible method dependent biases in the determination of radiation couplings.

2 Feedbacks and data description

2.1 Feedbacks

Feedback mechanisms are described as responses to changes in the radiative budget at the top of the atmosphere (TOA) due to external forcing processes (Thorsen et al. 2018).

In general the climate system can be visualized as a box, with TOA as box edge, in which physical laws like energy conservation apply. Observed long enough, the climate system reaches equilibrium, when the TOA net radiation flux $R_{\mathrm{net}}(t \to \infty)$ reaches zero. Considering smaller time scales, the radiation flux differs from zero. This can be due to several external forcing processes ΔF, which increase or dampen energy transport in and out of the system. External forcings are for example changes in greenhouse gas concentration, surface albedo, aerosol composition or a changing solar radiation (Bony et al. 2006). The changes of the TOA radiative flux due to changes in surface temperature T_{S}, resulting in variation of processes depending on temperature, are defined as climate feedbacks, which occur to restore the equilibrium state within the climate system, leading to $\Delta R = \Delta F + \lambda \Delta T_{\mathrm{S}}$ (Thorsen et al. 2018). They can be quantified using a climate feedback factor λ_{X}, where X stands for a certain physical property of the climate system, like surface albedo A, temperature T, water vapor WV or clouds CL. The total feedback factor λ is the sum of all specific feedback factors, with additional separation of λ_{T} into the lapse-rate feedback λ_{LR}, describing the rate of temperature decrease with height and the Planck feedback λ_{PL}, depending on surface longwave (LW) emission (Klocke, Quaas, and Stevens 2013):

$$\lambda = \underbrace{\lambda_{\mathrm{T}}}_{=\lambda_{\mathrm{PL}}+\lambda_{\mathrm{LR}}} + \lambda_{\mathrm{WV}} + \lambda_{\mathrm{CL}} + \lambda_{\mathrm{A}}. \tag{1}$$

λ (in units of $\mathrm{W\,m^{-2}\,K^{-1}}$) is defined as the change of radiation ΔR depending on surface temperature change ΔT_{S} and can be approximated as follows:

$$\lambda = \frac{\partial R}{\partial T_{\mathrm{S}}} = \sum_{\mathrm{X}} \frac{\partial R}{\partial X}\frac{\partial X}{\partial T_{\mathrm{S}}} + \phi(\partial^2) \approx \sum_{\mathrm{X}} \lambda_{\mathrm{X}} = \sum_{\mathrm{X}} \frac{\partial R}{\partial X}\frac{\partial X}{\partial T_{\mathrm{S}}}, \tag{2}$$

with indicated interactions between different feedbacks $\phi(\partial^2)$ and individual feedback parameters λ_X (Klocke, Quaas, and Stevens 2013). The new equilibrium is reached when $\Delta R = 0$, with ΔT_S for the equilibrium state is referred to as equilibrium climate sensitivity (ECS). In the following study particularly the surface albedo, Planck, lapse-rate and water vapor feedback are analyzed to determine potential biases between the PRP and kernel method.

Surface albedo The albedo of a specific surface is generally defined as its fraction of incoming radiation, reflected by the surface. It strongly depends on land use, snow cover or ice shield thickness and extent. Those soil and water surface properties are coupled to atmospheric and oceanic dynamics due to latent heat or freshwater transports. A change in the outgoing surface radiation and, thus a change in surface albedo, occurs by transformation of the surface properties. Apart from changes in land use, this is mostly associated with changes in snow cover and ice shield thickness in the high latitudes, due to temperature changes. Surface properties can vary on a locally small scale, making the parametrization of the surface albedo a challenging factor within GCMs (Bony et al. 2006). The surface albedo feedback is considered to be the weakest one compared to the others listed below, with a model mean of $0.3 \pm 0.1\,\mathrm{W\,m^{-2}\,K^{-1}}$, estimated by the IPCC AR5 (Flato et al. 2013). It is a positive feedback, leading to rising surface temperature, due to increased CO_2 concentration (Cess et al. 1991; Randall et al. 1994) and hence intensifies polar amplification (Bony et al. 2006).

Planck The Planck feedback is a component of the temperature feedback and often referred to as 'zero feedback', since it represents the earth's LW emission to space only depending on T_S. The earth's emission can be described using the Planck blackbody radiation law where $R = \varepsilon\sigma T_S^4$ with emissivity ε and the Stefan-Boltzmann constant σ. Using this formulation, the Planck feedback parameter for the global mean surface temperature of 288 K can be obtained by $\lambda_{PL} = -4\varepsilon\sigma T_S^3 = -3.4\,\mathrm{W\,m^{-2}\,K^{-1}}$. It follows that for an increase in incoming radiation of $1\,\mathrm{W\,m^{-2}}$, the surface temperature increases by 0.294 K. For the multi-model mean of the IPCC AR5 the Planck feedback was estimated as $3.2 \pm 0.1\,\mathrm{W\,m^{-2}\,K^{-1}}$ (Flato et al. 2013). It is the strongest negative feedback reducing the effect of global warming.

Lapse-rate The lapse-rate describes the negative temperature change with altitude. It strongly affects the LW emission of the earth's atmosphere. The lapse-rate in tropical regions can be approximated by the moist adiabatic profile, since it is driven by convective processes (Boucher et al. 2013). In those regions, rising saturated air parcels condensate and release latent heat, which is partly compensated by adiabatic cooling. This leads to a small change of temperature with altitude, less energy absorption within the atmosphere and thus a strongly negative lapse-rate feedback. In extra tropical regions (or areas of sinking motion) the lapse-rate change is harder to approximate (Boucher et al. 2013), also because of larger temperature decrease with altitude. Hence, more energy is absorbed within the atmosphere compared to the Tropics, leading to a positive lapse-rate feedback resulting in an amplification of the greenhouse effect. The IPCC AR5 multi-model mean of the global lapse-rate feedback is $-0.6 \pm 0.4\,\mathrm{W\,m^{-2}\,K^{-1}}$, thus it is dominated by the tropical responses and reduces the effect of global warming due to increased CO_2 emission (Flato et al. 2013).

Water vapor The water vapor feedback estimated by the IPCC AR5 multi model mean to $1.6 \pm 0.3\,\mathrm{W\,m^{-2}\,K^{-1}}$ is the strongest positive climate feedback (Flato et al. 2013). In-

creased CO_2 emission enhances the earth's greenhouse effect, and thus global warming. Consequently, rising temperatures increase specific humidity and the ability of water uptake within the atmosphere. This physical process is based on the Clausius-Clapeyron equation which relates the saturation vapor pressure to temperature for fixed relative humidity. If constant relative humidity is supposed, it is assumed that changes in relative humidity are much smaller than changes in the saturation mixing ratio for water vapor. Therefore, changes in the specific humidity are predominantly driven by changing saturation water vapor mixing ratio (Boucher et al. 2013). For example, the saturation mixing ratio for water vapor increases almost exponentially with temperature depending on altitude with 6 to $10\,\%\,K^{-1}$ close to the surface and up to $17\,\%\,K^{-1}$ in higher altitudes (Boucher et al. 2013). An increased amount of water vapor in the earth's atmosphere, means an increased greenhouse gas concentration and consequently rising temperature.

2.2 Data

The Coupled Model Intercomparison Project (CMIP) is a collection of experimental data generated by different global climate models in a standardized format. The current phase 6 contains the Diagnostic, Evaluation and Characterization of Klima (DECK) experiments and the CMIP historical simulations, whereby the DECK experiments are done using specific forcings, boundary conditions, initialization procedures, minimum length of runs and provide a baseline for performing many of the CMIP6 experiments (Eyring et al. 2016). The selected model MPI-ESM-LR is a combination of the atmospheric general circulation model ECHAM6 (Stevens et al. 2013), the land model JSBACH (Reick et al. 2013) and the ocean general circulation model MPIOM (Jungclaus et al. 2013) including the model for marine biogeochemistry HAMOCC (Ilyina et al. 2013) in low resolution (LR). Compared to ECHAM5, ECHAM6 provides a new radiation scheme and albedo calculation, in which the short-wave (SW) scheme has been replaced by the SW rapid radiation transfer model GCMs depending on solar zenith angle over open water, melt points on sea ice and snow cover (Roeckner et al. 2012). The horizontal resolution of the used ECHAM6 is T63/1.9 ° and it is vertically divided in 47 hybrid sigma pressure levels. The multi-century Pre-Industrial Control simulation (*piControl*), a coupled atmosphere- and ocean circulation DECK experiment, is used as a control run. The CO_2 concentration is prescribed and the minimum period of calculation is 500 years, starting from 1850, representing the conditions before the industrial revolution. The abruptly quadrupling CO_2 simulation (*abrupt4xCO_2*) is used as the perturbed run. It is developed to characterize the climate system's response to greenhouse gas forcing and also part of the DECK experiments in CMIP6 (Eyring et al. 2016). Therefore, only the CO_2 concentration is abruptly quadrupled in 1850 compared to the *piControl* simulation and then held constant, while all other parameters stay the same as in the control run. Preprocessing of the CMIP6 data was done by calculating the monthly averages of the daily data associated with cloud forcing (CFday) and combining them with the remaining required variables from monthly atmospheric data (Amon) and monthly atmospheric chemistry and aerosol data (AERmon) in one data file, including a land-sea mask, a glacier mask, surface pressure and geopotential data.

3 Partial radiative perturbation method

The partial radiative perturbation PRP method is based on the assumption that the TOA radiation R can be calculated depending on several atmospheric variables that have a significant feedback on the earth's energy budget such as water vapor WV, temperature T, surface albedo A and cloud properties CL, leading to $R = R(WV,T,CL,A)$ (Wetherald and Manabe 1988). The TOA radiation is calculated in two directions using the ECHAM6 standalone radiation model developed by the Max Planck Institute for Meteorology (MPI-M) in Hamburg and the Deutsche Wetterdienst (DWD) in Germany. To derive the TOA radiative imbalance ΔR, R is calculated for two different climate states, a control climate simulation ($piControl$) and a perturbed climate state ($abrupt4x\mathrm{CO}_2$). For the forward direction R is calculated using all variables, except the one of interest from the control run. The variable of interest is instead taken from the perturbed run. For example the difference in TOA radiation for water vapor can be written as $\delta R_{\mathrm{WV_{fwrd}}} = R(WV_{\mathrm{pert}}, T_{\mathrm{ctrl}}, CL_{\mathrm{ctrl}}, A_{\mathrm{ctrl}}) - R(WV_{\mathrm{ctrl}}, T_{\mathrm{ctrl}}, CL_{\mathrm{ctrl}}, A_{\mathrm{ctrl}})$. Likewise, the backward PRP TOA radiation can be obtained by using only the variable of interest from the control run and the remaining variables from the perturbed run leading to $\delta R_{\mathrm{WV_{bwrd}}} = R(WV_{\mathrm{ctrl}}, T_{\mathrm{pert}}, CL_{\mathrm{pert}}, A_{\mathrm{pert}}) - R(wv_{\mathrm{pert}}, T_{\mathrm{pert}}, CL_{\mathrm{pert}}, A_{\mathrm{pert}})$ for water vapor. To minimize biases due to the assumption of temporal uncorrelation between all fields, the TOA radiation is averaged over both directions (forward and backward) leading to the two-sided PRP results (Eq. 3) (Colman and McAvaney 1997; B. Soden, Broccoli, and Hemler 2004).

$$\delta R_{\mathrm{X_{2sides}}} = \frac{\delta R_{\mathrm{X_{fwrd}}} - \delta R_{\mathrm{X_{bwrd}}}}{2}. \tag{3}$$

With $\overline{\Delta T_{\mathrm{S}}}$, the temporally and spatially averaged surface temperature change between both runs λ_{X} can be estimated as:

$$\lambda_{\mathrm{X}} = \frac{\partial R}{\partial X}\frac{\partial X}{\partial T_{\mathrm{S}}} \approx \frac{\delta R_{\mathrm{X}}}{\delta X}\frac{\delta X}{\overline{\Delta T_{\mathrm{S}}}}, \tag{4}$$

With $\overline{\Delta T_{\mathrm{S}}} = \langle T_{\mathrm{S_{4xCO2}}}(x,y,t) - T_{\mathrm{S_{piCrtl}}}(x,y,t)\rangle = 4.65\,\mathrm{K}$. The PRP method has the advantage of estimating the responses of specific variables on the TOA radiative imbalance leading to straightforward interpretable results. However, this method is highly computational expensive, since it requires a large amount of processing and memory capacity (B. Soden, Broccoli, and Hemler 2004; Block and Mauritsen 2013).

4 Radiative kernel method

Radiative kernels are implemented comparably to the PRP method. Instead of taking the relevant variable from the perturbed climate simulation, only an incremental change of the variable is implemented, depending on the direction of the radiative flux calculation (Held and Brian Soden 2000; Brian Soden and Held 2006). The radiative kernels K_{X} are defined as:

$$K_{\mathrm{X}} = \frac{\partial R_{\mathrm{X}}(x,y)}{\partial X} \approx \frac{\delta R_{\mathrm{X}}(x,y)}{\delta X}, \tag{5}$$

Whereby $\delta R_{\mathrm{X}} = R(X+\delta X, Y) - R(X,Y)$, depending on the incremental change in the variable of interest δX. For the water vapor kernel the amount of water vapor corresponding to a positive temperature change of 1 K is used to perturb the specific humidity of the control climate state and the amount of water vapor corresponding to a negative temperature change of 1 K is used to perturb the specific humidity of the perturbed climate state (B. J. Soden et al. 2008; Klocke, Quaas, and Stevens 2013). The surface albedo kernel is calculated using a change of 1% in the surface albedo, and the temperature kernels are computed by changing the Temperature by 1 K (B. J. Soden et al. 2008; Klocke, Quaas, and Stevens 2013). The different feedback parameters can then be calculated by multiplying the kernel with ΔX and dividing by $\overline{\Delta T_{\mathrm{S}}}$ (Sec. 3):

$$\lambda_{\mathrm{X}} = \frac{\overline{\delta R_{\mathrm{X}}(x,y)}}{\overline{\Delta T_S}} = \frac{\overline{K_{\mathrm{X}}(x,y)\cdot\Delta X(x,y)}}{\overline{\Delta T_S}}, \tag{6}$$

with $\Delta X(x,y,z,t) = X_{4\mathrm{xCO2}}(x,y,z,t) - X_{\mathrm{piCrtl}}(x,y,z,t)$, representing the respective change in X between the perturbed and control climate. Vertical resolved variables (e.g. water vapor or temperature) need to be perturbed in each altitude level and the results are vertically integrated, which is done by summing over the model levels:

$$\delta R_{\mathrm{X}}(x,y,z,t) = \sum_z \frac{\delta R_{\mathrm{X}}(x,y,z,t)}{\delta X(x,y,z,t)} \cdot \Delta X(x,y,z,t) = \sum_z K_{\mathrm{X}}(x,y,z,t)\cdot\Delta X(x,y,z,t). \tag{7}$$

In the case of temperature, this is done only within the troposphere, to mask out the effect of stratospheric adjustment (Tomassini et al. 2013). The pressure at tropopause level depending on latitude *lat* was approximated as $p(z_{\mathrm{trop}}) = 100\,\mathrm{hPa} + 200\,\mathrm{hPa}\cdot|lat|\cdot 90^{\circ -1}$.

5 Results and discussion

In the following chapter, the results of the feedback determination using the PRP and kernel method are presented, discussed and compared to former studies (tab. 1). First, the results of the differently performed temporal averages are analyzed to justify the application of a multiyear monthly average mean dataset. Backward calculations for the PRP as well as the kernel method are generally multiplied with -1 to make them comparable to calculations in forward direction. Fig. 1 shows the feedback factor results obtained for yearly data of monthly averages λ_{PRP} (green) and the multiyear monthly averages over 39 years $\lambda_{PRP_{39yrs}}$ (orange). The zonal distributions are similar and the largest differences can be obtained for the water vapor feedback with $\Delta\lambda_{2\mathrm{sides}} \approx 0.022\,\mathrm{W\,m^{-2}\,K^{-1}}$ (fig. 1d). Since the found differences are assumed to be small compared to the feedback factor results, the simplification was applied and the kernels were calculated using multiyear monthly averages.

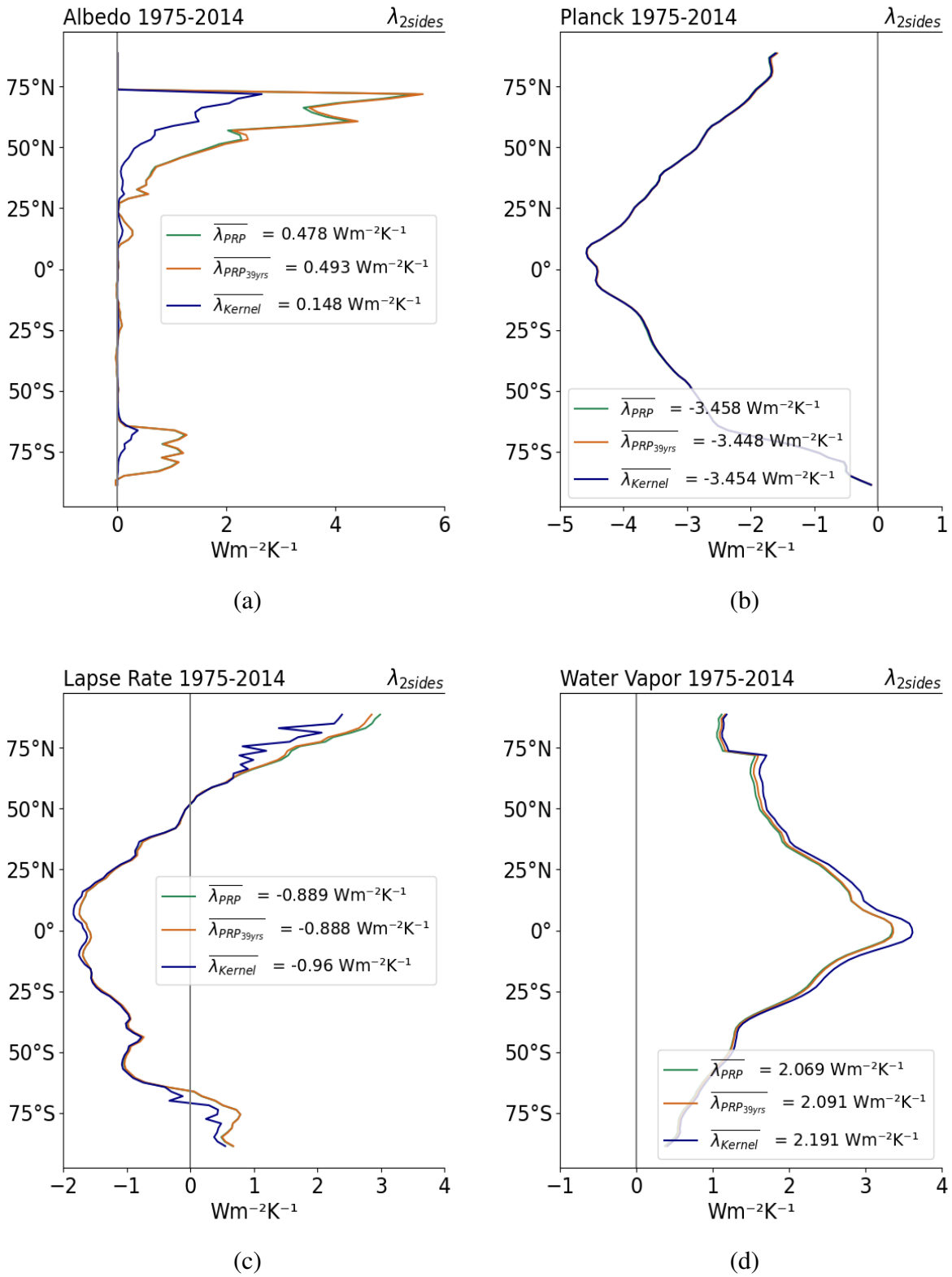

Figure 1: *Zonal averages of the individual feedback parameters for each year (green) and multiyear monthly averages (orange) using the PRP method and the results of the kernel method (blue), based on multiyear monthly averages. Including the surface albedo (a), Planck (b), lapse-rate (c) and water vapor (d) feedback in* $\mathrm{W\,m^{-2}\,K^{-1}}$ *based on multiyear monthly averages.*

Table. 1: *Comparison of resulting feedback parameters in* $\mathrm{W\,m^{-2}\,K^{-1}}$ *for the PRP and kernel method based on CMIP6 data and the MPI-ESM-LR model. Additionally, values of former studies of Klocke, Quaas, and Stevens (2013) based on ECHAM5 data, Rieger, Dietmüller, and Ponater (2017) and the IPCC AR5 kernel results for CMIP5 data and the MPI-ESM-LR model (Flato et al. 2013).*

Method	Direction	λ_A	λ_{PL}	λ_{LR}	λ_{WV}	$\sum\lambda$
PRP	forward	0.51	-3.693	-0.894	2.089	-1.988
	backward	0.475	-3.203	-0.882	2.092	-1.518
	two-sided	0.493	-3.448	-0.888	2.091	-1.752
Kernel	forward	0.199	-3.368	-0.804	1.701	-2.272
	backward	0.096	-3.541	-1.116	2.681	-1.88
	two-sided	0.148	-3.454	-0.96	2.191	-2.075
PRP Klocke et al. (2013)	forward	0.22	-3.23	-0.61	1.76	-1.86
	backward	0.16	-3.17	-0.23	1.79	-1.45
	two-sided	0.19	-3.23	-0.42	1.78	-1.68
Kernel Klocke et al. (2013)	forward	0.17	-3.08	-0.68	2.08	-1.51
PRP Rieger et al. (2017)	two-sided	0.23	-3.11	-0.86	2.01	-1.73
Kernel IPCC AR5 (2013)	forward	0.3	-3.3	-0.9	1.8	-2.1

5.0.1 Surface albedo feedback

The results of the 39-year average albedo feedback parameter (λ_A) calculations are shown as global distributions and zonal averages in fig. 1a and fig. 2. For both methods λ_A in units of $\mathrm{W\,m^{-2}\,K^{-1}}$ reaches its maximum value over land and sea ice in the polar regions. In lower latitudes and oceanic regions λ_A is close to zero. For the PRP method the forward calculation λ_{fwrd} with global averages of $0.51\,\mathrm{W\,m^{-2}\,K^{-1}}$ is slightly larger than the backward calculation λ_{bwrd} with $0.475\,\mathrm{W\,m^{-2}\,K^{-1}}$ (tab. 1). The two-sided PRP method yields a total albedo feedback of $0.493\,\mathrm{W\,m^{-2}\,K^{-1}}$. Forward and backward runs agree well. The kernel method with increased surface albedo of 1 % in the control run leads to a global average feedback parameter λ_{fwrd} of $0.199\,\mathrm{W\,m^{-2}\,K^{-1}}$. For decreased of surface albedo in the perturbed run, λ_{bwrd} is $0.096\,\mathrm{W\,m^{-2}\,K^{-1}}$, leading to a global average λ_{2sides} of $0.148\,\mathrm{W\,m^{-2}\,K^{-1}}$, which is displayed in fig. 5b. Comparing both methods as in fig. 1a, stronger results are retrieved with the PRP method than with the kernel approach. The kernel results are within the range of former studies, as listed in tab. 1, while the PRP results are larger than the outcomes of for example Klocke, Quaas, and Stevens 2013 and Rieger, Dietmüller, and Ponater 2017. Those disagreements could be due to differences in ECHAM6 compared to ECHAM5, used by Klocke, Quaas, and

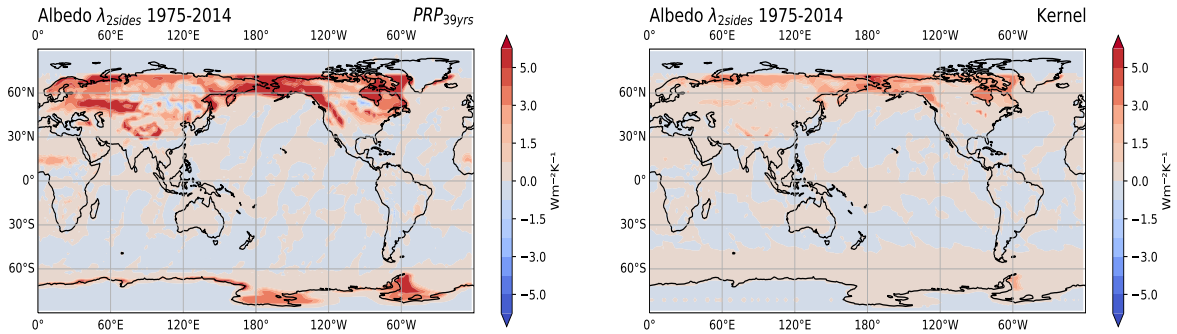

(a) (b)

Figure 2: *Comparison of the surface albedo feedback factor* λ_A *in* $\mathrm{W\,m^{-2}\,K^{-1}}$ *calculated using the PRP method (a) and the Kernel method (b). Spatially resolved as global distributions and based on multiyear monthly averages.*

Stevens 2013. Stevens et al. (2013) point out that in the radiation scheme of ECHAM6, the couplings between melt ponds and sea ice are not properly implemented, leading to and error dampening the effect of melt ponds. This artificially downsizes the surface albedo feedback. The results of Rieger, Dietmüller, and Ponater (2017) based on ECHAM6 data and the ECHAM6 radiation module retrieved a two-sided surface albedo feedback of $0.23\,\mathrm{W\,m^{-2}\,K^{-1}}$, which is closer to the feedback obtained in this study. The IPCC AR5 presents a surface albedo feedback of $0.3\,\mathrm{W\,m^{-2}\,K^{-1}}$ for a forward kernel calculation based on MPI-ESM-LR data, which is larger than the forward kernel results in this work ($0.199\,\mathrm{W\,m^{-2}\,K^{-1}}$). The same can be stated for the results of Block and Mauritsen (2013) with $0.48 \pm 0.03\,\mathrm{W\,m^{-2}\,K^{-1}}$. This leads to the assumption that the kernel method in this study generally underestimates the surface albedo feedback, which could be due to its high local variability or the implementation bug in the ECHAM6 radiation module, as described in Stevens et al. (2013), which strengthening the underestimation of the surface albedo feedback. The kernel method uses additionally a stronger linearization than the PRP method, assuming a linear change of the surface albedo with ΔT_S by 1%. Since the surface albedo depends on several factors, such as geometric pattern of the snow surface, solar zenith angle or snow characteristics, its change is strongly non-linear (Pirazzini 2004). Small changes in surface temperature around the freezing point of water can lead to huge differences in albedo, while changes beyond this range won't cause such great difference. Difficulties in the parametrization of small scale differences in the surface properties as described in Sec. 2.1, causing large model differences lead to an uncertainty in the magnitude of the surface albedo feedback. Nevertheless, studies agree in its positive sign (Bony et al. 2006), which is also observed in this study.

5.0.2 Planck feedback

Fig. 3 shows the global distribution of the Planck feedback parameter λ_{PL} and fig. 1b the zonal averages resulting from both methods. The two-sided PRP result λ_{2sides} is $-3.448\,\mathrm{W\,m^{-2}\,K^{-1}}$ with $\lambda_{fwrd} = -3.693\,\mathrm{W\,m^{-2}\,K^{-1}}$ and $\lambda_{bwrd} = -3.203\,\mathrm{W\,m^{-2}\,K^{-1}}$ (tab. 1). The kernel method yields a λ_{2sides} of $-3.454\,\mathrm{W\,m^{-2}\,K^{-1}}$.

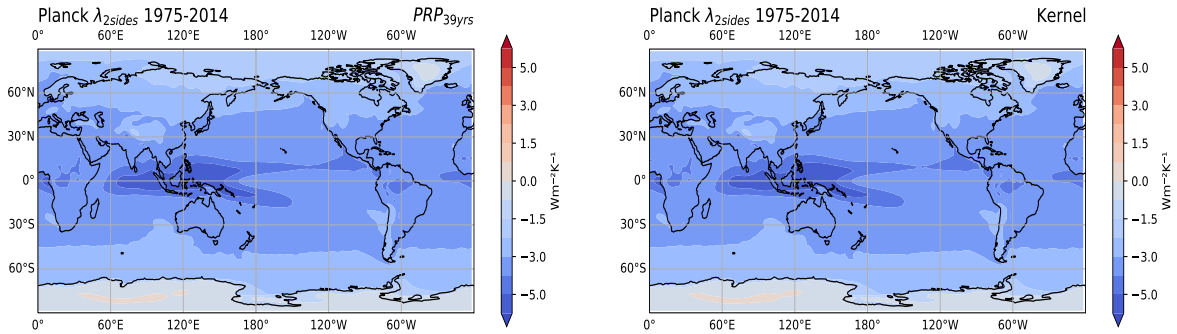

(a) (b)

Figure 3: *Comparison of the Planck feedback factor* λ_P *in* $\mathrm{W\,m^{-2}\,K^{-1}}$ *calculated using the PRP method (a) and the Kernel method (b). Spatially resolved as global distributions and based on multiyear monthly averages.*

The forward calculation, with an incremental increase of 1 K in the control run, gives slightly weaker results of $-3.368\,\mathrm{W\,m^{-2}\,K^{-1}}$ than the backward calculation, with a decrease of 1 K in the perturbed run $-3.541\,\mathrm{W\,m^{-2}\,K^{-1}}$ (tab. 1). The global distributions agree well with smallest values at the low latitudes where the surface temperature is lowest (fig. 3a and 3b). Comparing the two-sided PRP results to the results of Klocke, Quaas, and Stevens (2013) with $-3.23\,\mathrm{W\,m^{-2}\,K^{-1}}$ and Rieger, Dietmüller, and Ponater (2017) with $-3.11\,\mathrm{W\,m^{-2}\,K^{-1}}$, both show slightly weaker values for the Planck feedback. The same can be observed for the forward kernel results. The IPCC AR5 estimates the Planck feedback to $-3.3\,\mathrm{W\,m^{-2}\,K^{-1}}$ and Klocke, Quaas, and Stevens (2013) to $-3.08\,\mathrm{W\,m^{-2}\,K^{-1}}$. Although the results of the Planck feedback calculated using the PRP and kernel technique are slightly stronger than the Planck feedback estimated in former studies, they agree well with each other and the Planck feedback according to the Stefan-Boltzmann law. It is confirmed that the Planck feedback is the strongest negative feedback. Hence, it contributes significantly to LW cooling.

5.0.3 Lapse-rate feedback

Fig. 4 displays the global distribution of the lapse-rate feedback λ_{LR}. The geographical distributions of the Kernel and PRP calculations are generally similar and show minimal values for low latitudes and maximal values for high latitudes ranging from $-2.0\,\mathrm{W\,m^{-2}\,K^{-1}}$ to $4.0\,\mathrm{W\,m^{-2}\,K^{-1}}$ for the PRP method (fig. 4a) and $-2.0\,\mathrm{W\,m^{-2}\,K^{-1}}$ to $3.0\,\mathrm{W\,m^{-2}\,K^{-1}}$ for the kernel method (fig. 4b) with minimal values around Greenland. The zonal average for the forward PRP λ_{fwrd} of $-0.894\,\mathrm{W\,m^{-2}\,K^{-1}}$ is slightly larger than the average for the backward PRP λ_{bwrd} of $-0.882\,\mathrm{W\,m^{-2}\,K^{-1}}$ leading to the two-side PRP average $\lambda_{2\mathrm{sides}}$ of $-0.888\,\mathrm{W\,m^{-2}\,K^{-1}}$ as listed in tab. 1 . λ_{fwrd} for the temperature kernel with increased air temperature by 1 K gives an lapse-rate feedback of $-0.804\,\mathrm{W\,m^{-2}\,K^{-1}}$ and $-1.116\,\mathrm{W\,m^{-2}\,K^{-1}}$ for the perturbed climate state λ_{bwrd} with decreased T_{air} by 1 K. This yields to $\lambda_{2\mathrm{sides}}$ of $-0.96\,\mathrm{W\,m^{-2}\,K^{-1}}$. The comparison of both method results (fig. 1c) shows higher absolute values of the PRP technique compared to the kernel technique.

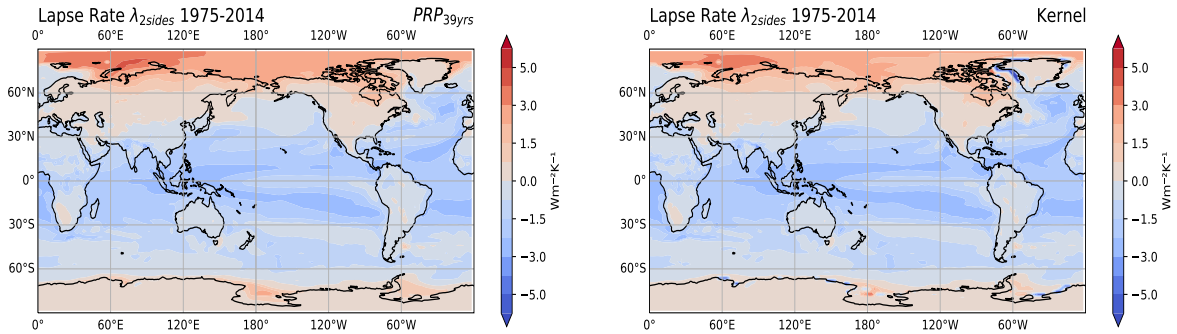

(a) (b)

Figure 4: *Comparison of the lapse-rate feedback factor* λ_{LR} *in* $\mathrm{W\,m^{-2}\,K^{-1}}$ *calculated using the PRP method (a) and the Kernel method (b). Spatially resolved as global distributions and based on multiyear monthly averages.*

The strongest variability is found in the polar regions using the kernel technique, leading to the assumption of more complex processes in those areas. Positive values of λ_{LR}, as observed in the extratropics (or areas of sinking motion) amplify the effect of global warming, due to an increased greenhouse effect (Held and Brian Soden 2000). Negative values of λ_{LR}, as observed in the Tropics, indicate a stronger decrease of temperature with height resulting in an increased LW emission back to space. The global average indicates a stronger tropical response than extra-tropical response, resulting in an overall negative lapse-rate feedback. Although the results of the PRP and kernel technique in this study agree well, there are slight differences to Klocke, Quaas, and Stevens (2013) with results of with $-0.42\,\mathrm{W\,m^{-2}\,K^{-1}}$ (tab. 1). A good agreement can be found for the PRP results of Rieger, Dietmüller, and Ponater (2017), who estimated $\lambda_{2\mathrm{sides}}$ to $-0.86\,\mathrm{W\,m^{-2}\,K^{-1}}$. Since Rieger, Dietmüller, and Ponater (2017) used the same dataset as in this study, this finding is not unexpected. For the forward kernel, the difference between Klocke, Quaas, and Stevens (2013) with an lapse-rate feedback parameter of $-0.68\,\mathrm{W\,m^{-2}\,K^{-1}}$ and this work with $-0.804\,\mathrm{W\,m^{-2}\,K^{-1}}$ is lower and comparable to the results of the IPCC AR5 with $-0.90\,\mathrm{W\,m^{-2}\,K^{-1}}$. Overall, the lapse-rate feedback compared to former studies using the same dataset, is slightly weaker for the kernel method and slightly stronger for the PRP method (tab. 1). The difference between both methods is largest in the high latitudes with stronger kernel results. This could be due to differences in surface warming and stronger coupling between the surface and free troposphere in the low latitudes compared to the high latitudes (Brian Soden and Held 2006). Since the temperature change with altitude within the troposphere can be approximated by $6.5\,\mathrm{K\,km^{-1}}$ (Held and Brian Soden 2000), a linearization is reasonable within the Tropics but needs further investigation for the extra Tropics.

5.0.4 Water vapor feedback

The water vapor feedback is displayed in fig. 5 with consistently positive values. The PRP and kernel global distribution do not differ much and have their maximum values in the equatorial region declining towards the poles, with minimal values in the Southern Hemisphere. The forward PRP yields to a feedback parameter of $2.089\,\mathrm{W\,m^{-2}\,K^{-1}}$ and

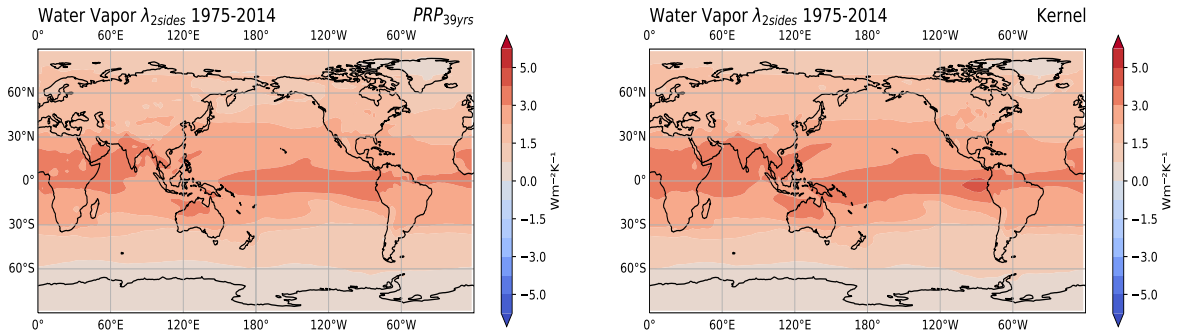

(a) (b)

Figure 5: *Comparison of the water vapor feedback factor* λ_{LR} *in* $\mathrm{W\,m^{-2}\,K^{-1}}$ *calculated using the PRP method (a) and the Kernel method (b). Spatially resolved as global distributions and based on multiyear monthly averages.*

the backward PRP to $2.092\,\mathrm{W\,m^{-2}\,K^{-1}}$ resulting in the two-sided PRP of $2.091\,\mathrm{W\,m^{-2}\,K^{-1}}$ (tab. 1). For the kernel method, the forward calculation, for which the specific humidity was increased by the amount corresponding to 1 K warming, differ more than the backward calculation, with decreased specific humidity corresponding to 1 K cooling. The global average for λ_{fwrd} gives $1.701\,\mathrm{W\,m^{-2}\,K^{-1}}$ and for λ_{bwrd} $2.681\,\mathrm{W\,m^{-2}\,K^{-1}}$, resulting in a two-sides kernel feedback parameter $\lambda_{2\mathrm{sides}}$ of $2.191\,\mathrm{W\,m^{-2}\,K^{-1}}$ (tab. 1). Since $\lambda_{2\mathrm{sides}}$ of the kernel method is similar to the PRP $\lambda_{2\mathrm{sides}}$ the decorrelation between both climate states by averaging over both directions seems reasonable. The current IPCC AR5 estimates the water vapor feedback factor to $1.8\,\mathrm{W\,m^{-2}\,K^{-1}}$ and Block and Mauritsen (2013) to $1.79 \pm 0.08\,\mathrm{W\,m^{-2}\,K^{-1}}$ for the MPI-ESM-LR and the forward kernel. These values are close to the forward kernel estimated in this study with $1.701\,\mathrm{W\,m^{-2}\,K^{-1}}$. The PRP results are within the same range as Rieger, Dietmüller, and Ponater (2017), as seen in tab. 1, but stronger than the results of Klocke, Quaas, and Stevens (2013). The water vapor feedback is the second strongest feedback. Furthermore, based on the Clausius-Clapeyron equation, the water vapor feedback is driven by changes in the saturation vapor pressure depending on temperature. An increase in global CO_2 concentration leads to rising global mean temperature, which in turn, enhances the ability of the atmosphere to take up water vapor. Since water vapor is a trace gas, more solar radiation is absorbed and the greenhouse effect is enhanced (Flato et al. 2013). Changes in specific humidity can be approximated by the change of saturation vapor pressure if relative humidity stays constant (Boucher et al. 2013). This yields to an exponential relationship between specific humidity and T_{S} according to the Clausius-Clapeyron relation. Even though the relation between surface temperature change and specific humidity change is not exactly linear, both linearizations (kernel and PRP) give reasonable results, compared to each other and to former studies.

6 Conclusion

Within this study, the determination of radiation couplings in climate change simulations has been analyzed using the PRP and kernel method based on MPI-ESM-LR data. The

results of the surface albedo, Planck, lapse-rate and water vapor feedback are within the range of previous studies and, hence, provide an example for the potential linearization of the feedback quantification. They also provide a general overview of regions strongly affected by an increased global CO_2 concentration. Furthermore, the effect of differently performed temporal averages has been investigated. It was found that the feedback factors calculated using a multiyear mean show only minimal differences to the results based on yearly data. This achievement provides the possibility to minimize computational expense. The strongest disagreement between both methods can be observed for the surface albedo feedback which is positive and the weakest among feedbacks (tab. 1). Since the surface albedo change is a strongly nonlinear process, especially in the temperature range of 260 K to 293 K in which the transition from ice covered surface to water takes place, the kernel technique generally underestimates the effect of the surface albedo feedback. This leads to less reliable model results compared to the more complex calculations of the PRP method. Regarding the Planck feedback, the strongest negative feedback, both methods agree well. It is slightly larger compared to former studies but corresponds to the Planck feedback of $-3.4\,\mathrm{W\,m^{-2}\,K^{-1}}$ for a global mean surface temperature of 288 K estimated from the Stefan-Boltzmann law. The lapse-rate feedback, which is on average negative, shows a fluctuation in polar regions using the kernel method. Apart from those, the PRP and kernel method results agree well and correspond to the IPCC AR5 results. It contributes to weakening of surface warming due to increased global CO_2 concentration. Both water vapor feedback results agree well with former studies. It is the strongest positive feedback, contributing to a temperature increase due to the strong greenhouse effect of water vapor. Despite the non-linear relationship between specific humidity and surface temperature, both methods give similar results and, thus, they are acceptable tools to determine the water vapor feedback. The disagreements between the forward and backward calculations for both methods are mostly compensated by the two-sided average. Thus, the application of both directions to minimize biases due to correlation within fields are found to be reasonable also for the kernel method. Once the kernels are calculated, they can be utilized for different climate perturbations without renewed radiative transfer calculations. This is a clear advantage of the kernel method. However, this advantage may compromise accuracy, as observed for the surface albedo and the lapse-rate feedback in polar regions. Decreasing computational effort due to the usage of multiyear monthly averages is possible. To receive more reliable results, the implementation bug in radiation scheme of ECHAM6 reported by (Stevens et al. 2013) needs to be corrected. Also, Polar regions must be given special attention, due to several complex coupling processes affecting the lapse-rate feedback. To confirm the results of this study further investigations are needed.

References

Block, K. and T. Mauritsen (2013). "Forcing and feedback in the MPI-ESM-LR coupled model under abruptly quadrupled CO2". In: *Journal of Advances in Modeling Earth Systems* 5, pp. 676–691. DOI: https://doi.org/10.1002/jame.20041.

Bony, Sandrine et al. (2006). "How Well Do We Understand and Evaluate Climate Change Feedback Processes?" In: *Journal of Climate* 19, pp. 3445–3482. DOI: 10.1175/JCLI3819.1.

Boucher, O. et al. (2013). "Clouds and Aerosols". In: *Climate Change 2013: The Physical Science Basis. Contribution of Working Group I to the Fifth Assessment Report of the Intergovernmental Panel on*

Climate Change. Ed. by T.F. Stocker et al., pp. 571–658. DOI: 10.1017/CBO9781107415324.016.

Cess, Robert et al. (1991). "Interpretation of Snow-Climate Feedback as Produced by 17 General Circulation Models". In: *Science (New York, N.Y.)* 253, pp. 888–92. DOI: 10.1126/science.253.5022.888.

Colman, R. A. and B. J. McAvaney (1997). "A study of general circulation model climate feedbacks determined from perturbed sea surface temperature experiments". In: *Journal of Geophysical Research: Atmospheres* 102, pp. 19383–19402. DOI: 10.1029/97JD00206.

Eyring, Veronika et al. (2016). "Overview of the Coupled Model Intercomparison Project Phase 6 (CMIP6) experimental design and organization". In: *Geoscientific Model Development* 9, pp. 1937–1958. DOI: 10.5194/gmd-9-1937-2016.

Flato, G. et al. (2013). "Evaluation of Climate Models". In: *Climate Change 2013: The Physical Science Basis. Contribution of Working Group I to the Fifth Assessment Report of the Intergovernmental Panel on Climate Change*. Ed. by T.F. Stocker et al., pp. 741–866. DOI: 10.1017/CBO9781107415324.020.

Held, Isaac and Brian Soden (2000). "Water Vapor Feedback and Global Warming". In: *Annual Review of Energy and The Environment* 25, pp. 441–475. DOI: 10.1146/annurev.energy.25.1.441.

Ilyina, Tatiana et al. (2013). "Global ocean biogeochemistry model HAMOCC: Model architecture and performance as component of the MPI-Earth system model in different CMIP5 experimental realizations". In: *Journal of Advances in Modeling Earth Systems* 5, pp. 287–315. DOI: 10.1029/2012MS000178.

Jungclaus, J. et al. (2013). "Characteristics of the ocean simulations in the Max Planck Institute Ocean Model (MPIOM) the ocean component of the MPI-Earth system model". In: *Journal of Advances in Modeling Earth Systems* 5. DOI: 10.1002/jame.20023.

Klocke, Daniel, Johannes Quaas, and Bjorn Stevens (2013). "Assessment of different metrics for physical climate feedback". In: *Climate Dynamics* 41. DOI: 10.1007/s00382-013-1757-1.

Pirazzini, Roberta (2004). "Surface albedo measurements over Antarctic sites in summer". In: *Journal of Geophysical Research: Atmospheres* 109. DOI: https://doi.org/10.1029/2004JD004617.

Randall, D. et al. (1994). "Analysis of snow feedbacks in 14 general circulation models". In: *Journal of Geophysical Research* 99, pp. 20757–. DOI: 10.1029/94JD01633.

Reick, C. et al. (2013). "Representation of natural and anthropogenic land cover change in MPI-ESM". In: *Journal of Advances in Modeling Earth Systems* 5. DOI: 10.1002/jame.20022.

Rieger, V.S., S. Dietmüller, and M. Ponater (2017). "Can feedback analysis be used to uncover the physical origin of climate sensitivity and efficacy differences?" In: *Climate Dynamics*. DOI: 10.1007/s00382-016-3476-x.

Roeckner, Erich et al. (2012). "Impact of melt ponds on Arctic sea ice in past and future climates by MPI-ESM". In: *Journal of Advances in Modeling Earth Systems* 4. DOI: 10.1029/2012MS000157.

Soden, B., A. Broccoli, and R. Hemler (2004). "On the Use of Cloud Forcing to Estimate Cloud Feedback". In: *Journal of Climate* 17. DOI: 10.1175/1520-0442(2004)017<3661:OTUOCF>2.0.CO;2.

Soden, Brian and Isaac Held (2006). "An Assessment of Climate Feedbacks in Coupled Ocean–Atmosphere Models". In: *Journal of Climate* 19. DOI: 10.1175/JCLI3799.1.

Soden, Brian J. et al. (2008). "Quantifying Climate Feedbacks Using Radiative Kernels". In: *Journal of Climate* 21, pp. 3504–3520. DOI: 10.1175/2007JCLI2110.1.

Stevens, Bjorn et al. (2013). "Atmospheric component of the MPI-M Earth System Model: ECHAM6". In: *Journal of Advances in Modeling Earth Systems* 5, pp. 146–172. DOI: 10.1002/jame.20015.

Thorsen, Tyler J. et al. (2018). "Observation-Based Decomposition of Radiative Perturbations and Radiative Kernels". In: *Journal of Climate* 31, pp. 10039–10058. DOI: 10.1175/JCLI-D-18-0045.1.

Tomassini, Lorenzo et al. (2013). "The respective roles of surface temperature driven feedbacks and tropospheric adjustment to CO2 in CMIP5 transient climate simulations". In: *Climate Dynamics* 41. DOI: 10.1007/s00382-013-1682-3.

Wetherald, R. T. and S. Manabe (1988). "Cloud Feedback Processes in a General Circulation Model". In: *Journal of Atmospheric Sciences* 45, pp. 1397–1416. DOI: 10.1175/1520-0469(1988)045<1397:CFPIAG>2.0.CO;2.